INTERNATIONAL ATOMIC ENERGY AGENCY
UNITED NATIONS EDUCATIONAL, SCIENTIFIC AND CULTURAL ORGANIZATION
INTERNATIONAL CENTRE FOR THEORETICAL PHYSICS
I.C.T.P., P.O. BOX 586, 34100 TRIESTE, ITALY, CABLE: CENTRATOM TRIESTE

UNITED NATIONS INDUSTRIAL DEVELOPMENT ORGANIZATION

INTERNATIONAL CENTRE FOR SCIENCE AND HIGH TECHNOLOGY
c/o INTERNATIONAL CENTRE FOR THEORETICAL PHYSICS 34100 TRIESTE (ITALY) VIA GRIGNANO, 9 (ADRIATICO PALACE) P.O. BOX 586 TELEPHONE 040-224572 TELEFAX 040-224575 TELEX 460449 APH I

H4.SMR/540-4

Second Training College on Physics and Technology of Lasers and Optical Fibres

21 January - 15 February 1991

Experimental Feasibility of the Airborne Measurement of Absolute Oil Fluorescence Spectral Conversion Efficiency

Frank E. Hoge
NASA Goddard Space Flight Center
Wallops Island, Virginia, USA

Experimental feasibility of the airborne measurement of absolute oil fluorescence spectral conversion efficiency

F. E. Hoge and R. N. Swift

a reprint from **Applied Optics**
volume 22, number 1, January 1, 1983

Experimental feasibility of the airborne measurement of absolute oil fluorescence spectral conversion efficiency

F. E. Hoge and R. N. Swift

Recent theoretical work has shown conceptual feasibility for the airborne measurement of the absolute oil fluorescence spectral conversion efficiency (AOFSCE) of crude and refined petroleum oils on the ocean surface without *a priori* knowledge of the film thickness. Reported herein are airborne lidar oil spill experiments conducted to determine the practical feasibility of the AOFSCE computational model. The results of these investigations demonstrate that the AOFSCE model is practical over a considerable range of oil film thicknesses provided the fluorescence efficiency of the oil does not approach the minimum detection sensitivity limitations of the lidar system. Separate airborne lidar experiments to demonstrate measurement of the water column Raman conversion efficiency have also been conducted to ascertain the ultimate feasibility of converting such relative oil fluorescence to absolute values. The AOFSCE model shows excellent potential, however, further airborne water column Raman conversion efficiency experiments with improved temporal or depth-resolved waveform calibration and software deconvolution techniques are required for final feasibility determination.

I. Introduction

Each year millions of liters of crude and refined petroleum oil are spilled or pumped into the world's oceans. Except for spills of catastrophic proportions the activities of the transporting oil tankers largely go unnoticed. It is apparently during routine day-to-day operations that most oil is released into the oceans.[1] Granted some natural seepage of crude oil occurs but these quantities are small. It is believed by many governments that the release of oil by tankers could be significantly reduced if good scientific and legally acceptable methods of monitoring and identifying the discharge could be developed. The fingerprinting of surface oil by laser-induced fluorescence is a promising method that has been under study by various countries for the past decade.[2–4]

Early airborne lidar development and field experiments in the U.S. were reported by Fantasia and Ingrao.[5,6] They also reported the laboratory measurement of the conversion efficiency (unitless power ratio) of a large number of petroleum oils. The absolute oil fluorescence conversion efficiency concept was introduced by Horvath *et al.*,[7] and spectral data were measured and presented for several general oil types. The concept of applying the oceanic water Raman backscatter for the calibration of absolute oil spectral fluorescence conversion efficiency (AOFSCE) was first introduced by Kung and Itzkan.[8] The feasibility of acquisition and practical utilization of the requisite airborne lidar field data for use with the Kung-Itzkan model is the subject of the investigations reported herein.

Investigators from the Canada Center for Remote Sensing (CCRS) reported the field trials of an airborne multichannel lidar fluorosensor.[9,10] More importantly they revealed a correlation technique which, when applied to the data, clearly allowed the differentiation of crude oil from a fluorescent dye release and the general fluorescence background (Gelbstoff) of the surrounding ocean water. Their correlation technique is applied to intensity-normalized spectral fluorescence data so that only the wavelength variations of the targets are discriminated. Thus, they could not spectrally differentiate between the two crude oils observed during their airborne field trials. As a practical consideration, they suggest that differentiation would be possible between the two oils if the ~10× absolute fluorescence conversion were considered. The AOFSCE technique can potentially allow a general classification of oils without any *a priori* knowledge of the oil film thickness or the spectral properties of the oil. Furthermore, the technique properly accounts for the background interference occurring in the spectra due to Gelbstoff or dissolved organic matter. It is believed that the AOFSCE

Frank Hoge is with NASA Wallops Flight Center, Wallops Island, Virginia 23337; R. N. Swift is with EG&G Washington Analytical Services Center, Inc., Pocomoke City, Maryland 21851.

Received 7 August 1982.

technique, while powerful in its own right, would be enhanced further if embedded within the framework of the O'Neil *et al.* correlation procedure.

The experimental results presented in this paper are intended primarily as a status report on our efforts to date in applying the AOFSCE technique to airborne laser fluorosensing data. The results indicate that the technique is feasible over a range of oil thicknesses provided the fluorescence of the oil is within the sensitivity limits of the system. Our efforts to independently determine the Raman conversion efficiency of watermasses are also presented, however, system related problems have thus far prevented the successful implementation of this application of the NASA airborne oceanographic lidar (AOL). Improvements to system components to facilitate the measurement of optical transmission properties using water Raman backscatter have since been implemented and are discussed in the concluding section of this paper.

II. Theory

A method to calculate the characteristic infinite thickness absolute spectral fluorescence conversion efficiency from finite thickness oil films has been given by Kung and Itzkan.[8] The method applies to a laser transceiver utilized on a low-flying aircraft. The theory considers the use of the laser-induced water Raman backscatter cross section for the essential calibration of the oil fluorescence conversion. Furthermore, the usual interfering background fluorescence due to Gelbstoff is also handled by the theoretical development.

The absolute oil spectral fluorescence conversion efficiency η_f is given by[8]

$$\eta_f = \left(\frac{\sigma N_w T_e T_r}{\alpha_e + \alpha_r}\right) \cdot \left(\frac{\theta_f}{1 - \Delta_r^{1+\varepsilon}}\right) \cdot \left(1 - \frac{\Delta_r^{1+\varepsilon}}{\Xi_f}\right), \tag{1}$$

where σ = Raman cross section of water,
N_w = number density of water,
T_e, T_r = transmissivities of the air–sea interface at the laser emission and Raman wavelengths, respectively,
α_e, α_r = extinction or beam attenuation coefficient of seawater at the laser emission and Raman wavelengths, respectively,
θ_f = oil fluorescence signal at wavelength λ_f as normalized by the water Raman signal measured outside the slick, K_f/R,
Δ_r = Raman signal amplitude measured while over the oil slick with fluorescence contributions from the oil and Gelbstoff at λ_r removed by interpolation and subtraction, R'/R, Fig. 1, and
Ξ_f = oil fluorescence measured over the oil slick normalized or divided by the fluorescence signal at λ_f observed outside the slick, K_f/J_f.

Finally,

$$\varepsilon = \frac{\kappa_f - \kappa_r}{\kappa_e + \kappa_r}, \tag{2}$$

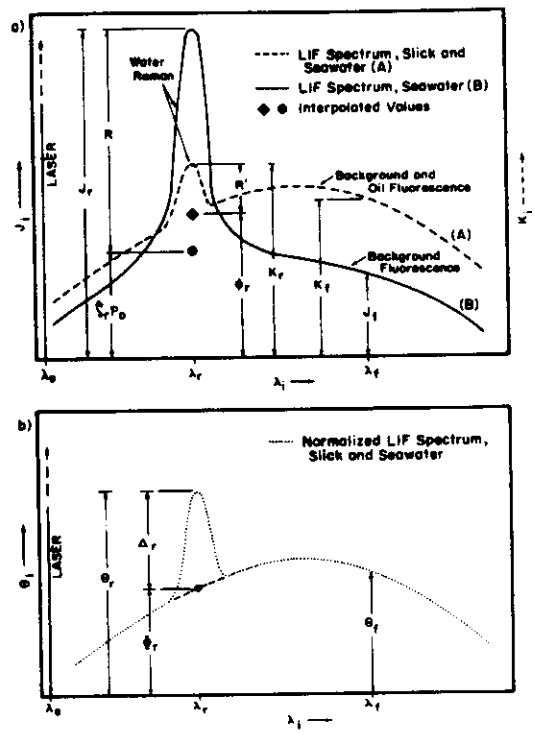

Fig. 1. (a) Theoretical or expected laser-induced fluorescence spectral waveforms over (*A*) ocean water covered by an optically thin oil film and (*B*) ocean water. (b) Spectral waveform of ocean water normalized by water Raman backscatter *R*.

where κ_f, κ_r, and κ_e are the extinction coefficients of the oil at wavelengths λ_f, λ_r, and λ_e, respectively. Figure 1 contains the essential definitions of many of the above parameters defined for laser-induced fluorescence (LIF) of oil and water column constituents.

The first multiplicative term in Eq. (1) is known as the seawater Raman conversion efficiency:

$$\psi = \frac{\sigma N_w T_e T_r}{(\alpha_e + \alpha_r)}. \tag{3}$$

Thus, a straightforward or simplified interpretation of Eq. (1) is that the absolute oil fluorescence spectral conversion efficiency is the water column Raman conversion efficiency modified by two additional multiplicative terms whose values depend on the extinction and spectral fluorescence properties of the oil. Ideally, the oil fluoresensing lidar can be equipped to remotely measure the sum of the extinction coefficients of water, $\alpha_e + \alpha_r$, by utilizing the temporal variation of the Raman signal within the water column.[8] Then

$$\alpha_e + \alpha_r = \frac{\sigma \tau}{2n}, \tag{4}$$

where c is the velocity of light, n is the index of refraction, and τ is the Raman signal decay time constant computed from total elapsed or two-way time decay data. During our oil spill experiments, the NASA AOL could not be rapidly reconfigured from the spectral mode to the temporal mode. Thus, for our oil fluorescence portion of this work we will use an estimate of ψ from the water optical transmission data taken by truth

ships in the immediate vicinity of the spill. We recognize that the ultimate utility of AOFSCE for the general typing of oil spills with an airborne laser fluorosensing system will require a measurement of ψ independent of any supporting surface vessels. Therefore, the latter sections of this paper will describe our progress to date in the measurement of ψ during a separate field experiment. The reader will no doubt recognize the general oceanographic usefulness of the remote measurement of ψ and its interpretation via Eq. (3) of the extinction coefficient of the water column. These field experiments were performed with this oceanographic utility in mind.

A determination of the optical attenuation properties of the watermass at the oil spill test site was to have been made from the truthing vessel with an onboard beam transmissometer. Because of operational problems, however, only Secchi disk readings were available for our analysis. To estimate the beam attenuation coefficient of the water, we equated the results of Holmes[11] with those of Shannon[12] and Ofelt[13] to yield

$$\frac{1.44}{Z_D} = 0.2\alpha + 0.04, \tag{5}$$

where Z_D is the Secchi depth and α is the beam attenuation coefficient. The numerical results obtained from using Eq. (5) are not greatly different from the results of Gordon and Wouters.[14] In fact for the Secchi depths we encountered there is <20% difference between Eq. (5) and the Gordon and Wouters results. The reader will note that it has been assumed that the extinction coefficient of seawater as required by the Kung and Itzkan fluorescence conversion efficiency theory is indeed the beam attenuation and not the diffuse attenuation coefficient. The use of classical beam and diffuse attenuation coefficients in support of or in combination with lidar measurements is a controversial subject when oceanographic lidar workers congregate. Bristow *et al.*[15] have shown that the laser-induced water Raman backscatter and beam attenuation are very highly correlated in fresh water (Lake Mead). Furthermore, normalization of the chlorophyll *a* response band with the water Raman backscatter signal ultimately leads to an accurate measurement of chlorophyll *a*. Other lidar workers concerned with bathymetry[16] have essentially shown that backscattered signal strength and depth error are due in large part to the optical depth. Furthermore, recent Monte Carlo modeling results by Gordon[17] have revealed that the ratio of the radius of the spot on the sea surface viewed by the lidar receiver to the mean free path of the photons in the water column is a significant parameter. For values of this parameter near zero a lidar system with a limited field of view will measure a quantity that approaches the beam attenuation coefficient. The lidar measurement will approach the attenuation coefficient for downwelling irradiance for cases where the mean free path is much less than the radius of the spot at the sea surface. Essentially similar modeling results were recently obtained by Poole and Esaias.[18] Accordingly we will herein assume that the extinction coefficient of seawater described by Kung and Itzkan is the beam attenuation coefficient since our transmit beam diameter was ≤0.5 m in these experiments in which the Secchi disk depth was found to be 9.1 m during the 3 Nov. 1978 LaRosa crude mission. No Secchi reading was available for the 9 Nov. 1978 Murban crude spill. The latter airborne mission revealed a Raman backscatter which was 1.5 times higher than on 3 Nov. Accordingly, the beam attenuation was decreased by this factor for the 9 Nov. data analysis. The experimental justification for this correction is based on the work by Bristow *et al.*[15] Solving Eq. (5) for α yields

$$\alpha = \frac{7.2}{Z_s} - 0.2. \tag{6}$$

Admittedly, this equation will give some sizable standard errors of estimate.[11] However, the airborne absolute oil fluorescence conversion efficiency technique demands only measurements having an approximate accuracy of 50%.[8] Furthermore, as we shall show, the feasibility of the oil portion of the AOFSCE measurement technique is believed to be adequately demonstrated in spite of the potentially large errors in estimating ψ, the water Raman conversion efficiency used for the absolute calibration.

But $\alpha_e + \alpha_r$ is required in Eq. (1). Within the experimental errors introduced by Eq. (5), set $\alpha_e + \alpha_r = 2\alpha$. Then the seawater Raman conversion efficiency is

$$\psi = \frac{\sigma N_w T_e T_r}{2\left(\frac{7.2}{Z_s} - 0.2\right)}. \tag{7}$$

The OH-stretch, 3300-cm^{-1} Raman backscattering cross section for liquid water, σ, has been measured by Slusher and Derr[19] and also by Chang and Young[20] for the entire band. A value of 4.5×10^{-29} cm^2/molecule · sr is given for 488 nm in Ref. 20 and will be used herein with appropriate corrections for wavelength. The cross section σ at 337.1 nm may be estimated from[20]

$$\sigma_{337} = \sigma_{488}\left(\frac{\nu_{337} - \nu}{\nu_{488} - \nu}\right)^4, \tag{8}$$

where σ_{488} = Raman scattering cross section at 488 nm,

ν_{337}, ν_{488} = wave numbers corresponding to wavelengths of 337.1 and 488.0 nm in units of cm^{-1}, and

ν = water Raman OH-stretch frequency shift (3300 cm^{-1}).

Or

$$\sigma_{337} = (5.531)\sigma_{488}. \tag{9}$$

The number density of water N_w is 3.3×10^{22} molecules/cm^3. Then the $\sigma_{337} N$ product is 8.28×10^{-5} $m^{-1} \cdot sr^{-1} \cdot nm^{-1}$. A full-power Raman bandwidth of 30.3 nm was extracted from the liquid water spectrum (2800–3700 cm^{-1} for 488-nm excitation) given in Ref. 19. An air–water transmissivity of $T_e = T_r = 0.98$ will be used. For a Secchi disk depth of 9.1 m, Eq. (7) yields $\psi = 2.2 \times 10^{-5}$ $sr^{-1} \cdot nm^{-1}$. This is the value that will be subsequently used in our calculations.

III. Instrument Description

The field experiments were performed with the NASA airborne oceanographic lidar (AOL). The AOL is a conically scanning laser radar having three basic modes of operation: (1) fluorosensing, (2) bathymetry, and (3) ranging.

The fluorosensing mode utilizes a 40-channel transmission grating/photomultiplier tube array to resolve the laser-induced fluorescence from targets of interest. The AOL instrument is configured to accept different laser transmitters and has been used for airborne oil film thickness,[21] dye concentration,[22] and chlorophyll *a*/photosynthetic pigment[23,24] measurements. The fluorosensing mode was used for the airborne spectral measurements described herein. The range of AOL transmitter and receiver parameters used in the oil spectral measurements is essentially described in some previous publications.[21,22] For convenience, the important parameters are summarized in the fluorosensor portion of Table I.

The bathymetric mode of the AOL utilizes up to forty sequentially time-gated analog-to-digital converters (charge digitizers) to record backscattered signals as a function of depth. When used to observe the on-wavelength backscatter, the system essentially functions as a lidar bathymeter.[25] For our depth-resolved Raman measurements, an interference filter centered on the water Raman band was used to select the proper wavelength and reject the laser backscatter. A long pass filter was used in series with the interference filter to provide additional rejection of the on-wavelength Fresnel and Mie backscatter. The important system instrumentation parameters are summarized in the Raman portion of Table I for the depth-resolved temporal experiments.

The ranging mode of the AOL is essentially a time-of-flight intervalometer which measures the combined round trip time of the transmitted and resultant backscattered pulse from the surface and upper water column. More importantly this mode provides the timing synchronization for activation of components to digitize and record the laser-induced fluorescence returns or the water column backscatter in the respective fluorosensing and bathymetric modes operation. Accordingly, the ranging mode must always operate before any other modes can function.

Table I. AOL Operating Parameters

	Oil fluorosensing mode	Depth-resolved Raman
Transmitter	Nitrogen laser	Excimer-pumped dye
Wavelength	337.1 nm	308/422.6
Bandwidth	0.1 nm	<1 nm
Pulse width	10 nsec	5 nsec
Pulse rate	≤100 Hz	25 Hz
Peak output power (max)	100 kW	700 kW
Beam divergence	4 mr	4 mr
Receiver		
Bandwidth	3500–8000 Å	8 nm at 493.5 nm plus Kodak No. 4 blocking
Spectral resolution (min)	11.25 nm	
Field of view	1–20 mr, variable, vertical and horizontal	5 mr
Temporal resolution	8–150 nsec, variable	2.5 nsec, 36 channels
Experiment		
Aircraft altitude	150 m	150 m
Aircraft velocity	75 m/sec	100 m/sec
Measurement background	Day	Day

IV. Results

A. Oil Fluorescence Field Experiments

During November 1978 the AOL participated in a series of missions designed to measure the effects of a dispersant on the spreading rates of crude oils spilled on the ocean surface.[26,27] The test site was located ~64 km (~40 miles) SE of Sandy Hook, N.J., in water having depths >40 m. The overall coordination of spill, airborne, and ocean surface measurements was handled jointly by personnel from JBF Scientific Corp. and NASA Langley Research Center (LaRC).

The AOL missions were flown onboard a NASA Wallops C-54 aircraft together with the Naval Research Laboratory 22- and 31-GHz scanning microwave radiometer[27] which was operated by LaRC personnel. Other instrumentation onboard the Wallops aircraft during both series of missions included a 70-mm Hasselblad camera, a 35-mm flight research camera, and a TV camera with a video tape recorder. Additional airborne observations from other aircraft were made by the Canadian Center for Remote Sensing (CCRS) and JBF Scientific Corp. Shipborne measurements were performed from the research vessel Annandale operated by the Marine Science Consortium, Inc. and from the National Oceanic and Atmospheric Administration (NOAA) vessel Kelez. Some results from the CCRS fluorosensor[9] and the NASA AOL[21] were reported previously. A paper providing an overall assessment of the effects of the dispersants on oil spreading characteristics using the AOL and NRL scanning microwave systems along with surface observations has been submitted[27] and a report on the combined airborne instrumentation is currently in preparation.

The general scenario of the oil spill experiment has been described in detail[9,21,26,27] and will be briefly discussed here for purposes of continuity and completeness. As approved by the Environmental Protection Agency (EPA), four separate crude oil slicks were deployed by pumping the oil onto the ocean surface from the research vessel Annandale. Two of the spills were made with Murban, a light Middle East oil, and two with LaRosa, a heavy Venezuelan oil. One of the spills from each of the oils was treated with a dispersant within 10 min after deployment and the other was allowed to age for ~2 h before the application of the dispersant from a helicopter. Information regarding the

spills is provided in Table II. Additional physical characteristics of the two crude oils are given in Table III. The data analyzed for this paper were from missions flown over the LaRosa slick on 3 Nov. 1978 and the Murban slick on 9 Nov. 1978.

The airborne spectra were processed using techniques described previously in detail.[8,21] For the measurement of oil film thickness this process involves removing unwanted background fluorescence (Gelbstoff) and normal oil fluorescence from the Raman spectral band by interpolation. For oil conversion efficiency measurements the Gelbstoff and normal oil fluorescence are removed from the Raman band in an identical manner. Background or Gelbstoff fluorescence occurring in other oil spectral fluorescence bands are accounted for in the third multiplicative term of Eq. (1). The removal of Gelbstoff fluorescence can be a significant problem in nearshore or estuarine areas with high volumes of entrained organic matter. Our observations made within the test site but outside of the spill itself yielded rather monotonous spectra with very low Gelbstoff fluorescence. This minor amount of Gelbstoff fluorescence was removed from the Raman band with an interpolation technique to be discussed. The contribution of fluorescence from the LaRosa oil at the 381-nm water Raman backscatter line was below the detection limits of the AOL at the time the 1978 experiment was performed. The detection limit of the AOL at ~500 nm will be discussed at length in a subsequent section. As will be seen, the uncorrected Raman backscatter signal was observed to consistently depress completely over the optically thick region of the LaRosa slick indicating no measurable fluorescence signal from the oil itself at the Raman wavelength. In data obtained over the more highly fluorescent Murban oil slick, however, the uncorrected Raman signal did not depress below ~200 counts and was observed to increase somewhat above this minimum over the optically thick portions of the slick. Ideally, interpolation through the channel containing the Raman signal from surrounding channels on both sides of the Raman channel would satisfactorily remove the oil fluorescence contribution.[8] During this initial experiment with the AOL over an oil spill the system's fluorosensor was equipped with a rigidly mounted folding mirror which placed the Raman band between channels 2 and 3. A small amount of Raman signal was also found in channel 1 thus making interpolation difficult. We therefore extrapolated a slope from channels 4 and 5 through channel 2 to obtain the corrected Raman backscattered signal. Recent improvements in the AOL, which will be discussed in the concluding section of the paper, will allow the more straightforward and reliable interpolation approach to resolving this problem.

Figures 2 and 3 are cross-sectional plots of data obtained on Pass 2 during an overflight of the LaRosa spill and on Pass 4 over the Murban spill, respectively. These graphs illustrate typical data obtained from each of the oil spills and will serve as a reference in the ensuing discussion of absolute oil fluorescence spectral conversion efficiency. These data have not been edited or filtered in any way. At the nominal aircraft velocity of 85 m/sec these profiles represent a horizontal distance of ~127 m. Both of these passes were flown early in their respective experiments, thus the cross-sectional diameters of the slicks in the downwind direction were >100 m. On passes made later in time on both missions considerable spreading was observed, especially in the downwind direction. The pass over the LaRosa slick shown in Fig. 2 was flown prior to the addition of the dispersant, while the pass over the Murban slick shown in Fig. 3 was flown within 20 min after the addition of the dispersant. The first three passes over the Murban slick were taken when the diameter was quite small thus relatively few data points were available for analysis. Since we were unable to detect any noticeable effect of the dispersant in the airborne spectral fluorescence data, Pass 4 made over the enlarged slick was selected for presentation in this document. The profiles in both figures designated (a) are the corrected Raman backscattered signal plotted against time for a short segment of the flight line in the vicinity of the oil spill. Likewise, those profiles labeled (b) are the corrected peak fluorescence responses for channel 12 centered at 500 nm. Both of these profiles are plotted in counts from the charge digitizers in the AOL data acquisition system. The third profile, designated (c) in the figures, is the oil slick thickness determined by the Raman depression technique.[21]

The water Raman backscatter profile for both of the oil types depressed as the slick was encountered and returned to the same level after the slick was passed. As previously mentioned, contributions of fluorescence from the Murban crude oil were removed from the Raman signal, thus both Raman profiles can be seen to depress completely (to 1 digital count) over portions of the slicks that were optically thick. There are a number

Table II. Experiment and Data Summary

Date	Crude oil type	Dispersant applied	AOL data passes before dispersant nonscan	AOL data passes before dispersant scanning	Total AOL data passes
2 Nov. 1978	Murban	After 2 h	0	0	18
3 Nov. 1978	LaRosa	After 2 h	3	5	33
9 Nov. 1978	LaRosa	Immediately	0	0	37
9 Nov. 1978	Murban	Immediately	0	1	17

Table III. Spilled Oil Types and Selected Physical Characteristics

Oil	Source	Type crude	Fluorescence		Extinction coefficient (nm^{-1})			
			Emission	Peak wavelength (nm)	337.1 nm	381 nm	500 nm	API°
LaRosa	Venezuela	Heavy	Low	490	896	434	189	23.3°
Murban	Middle East	Light	High	505	265	95	26	38.1°

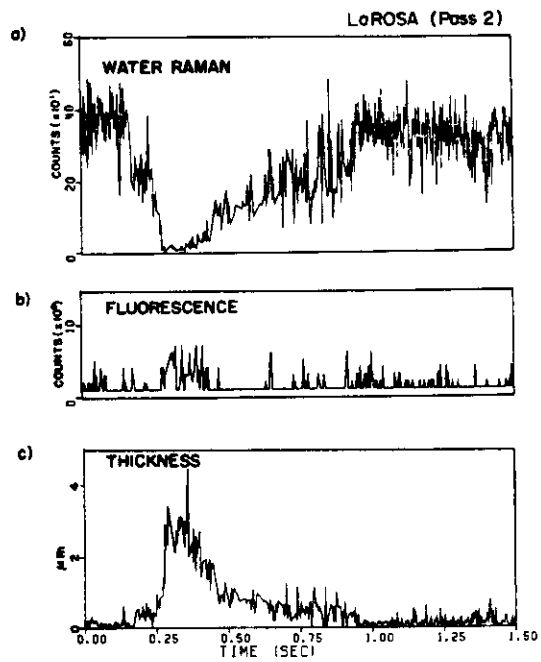

Fig. 2. (a) Water Raman backscatter and (b) oil fluorescence signals obtained over the LaRosa oil slick. (c) The computed thickness using the data in (a) and the extinction coefficients from Table III.

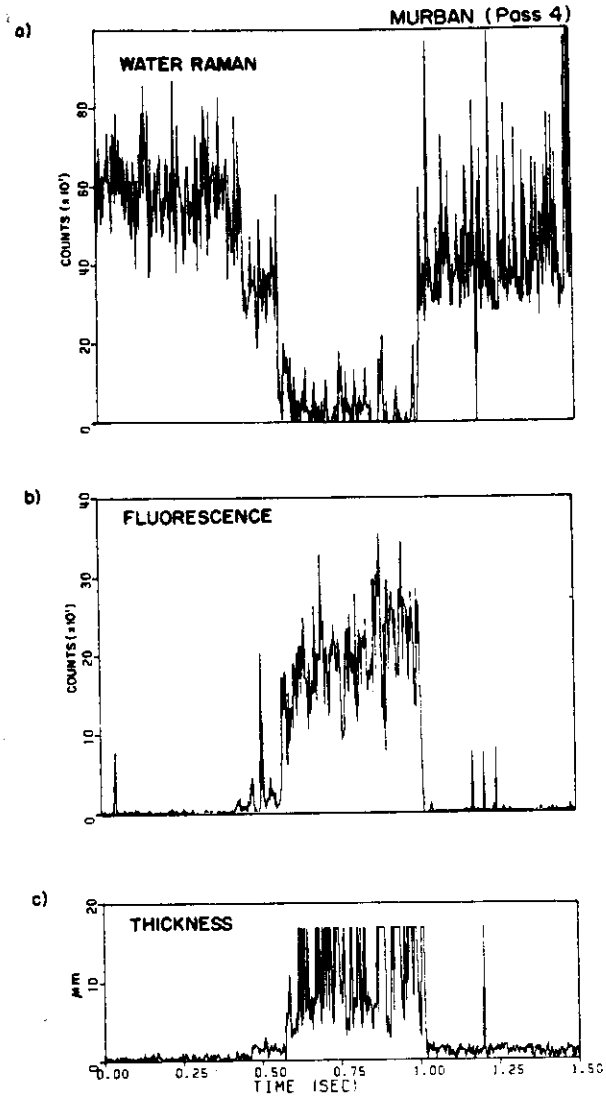

Fig. 3. (a) Water Raman backscatter and (b) oil fluorescence signals obtained over the Murban oil slick. (c) The computed thickness using the data in (a) and the extinction coefficients from Table III.

of places on both profiles over the slick where missing data points can be seen, especially over the Murban slick in Fig. 3. These dropouts occur when the power in the surface return energy at the laser wavelength is of insufficient strength to trigger the digitization of the fluorescence spectral signals. Presumably the reduction of the laser return signal strength is due to a combination of the damping of the capillary wave structure by the oil film accompanied by increased non-nadir forward scatter as well as by absorption of laser energy by the oil. Likewise, as will be subsequently discussed, a considerable decrease in the modulation of the return signal of the Raman backscatter profiles is evident over the slick. A substantial increase in the Raman backscatter signal strength can be seen when the Raman profile from 3 Nov. in Fig. 2(a) is compared with its counterpart from 9 Nov. in Fig. 3(a) indicating that an increase in the water column optical transmission had occurred between the two missions. There was however no notable change in the background Gelbstoff fluorescence between the two missions accompanying the change in water clarity.

The fluorescence conversion efficiencies between the two oils as observed in the aircraft data are different by a factor of more than 10× as is evident when the two fluorescence profiles are compared (see Figs. 2 and 3). Please note that the scale of the Y axes for the individual profiles has been appropriately chosen for fluorescence and thickness to reflect the magnitude of changes in these parameters on the respective plots. The weakly fluorescing LaRosa oil shows a detectable return at 500 nm only over the very thickest portion of the oil spill, while the Murban oil yielded discernible responses over practically the entire area where the Raman backscatter depression is evident. This aspect will be discussed further in the description of the AOFSCE results later in this section.

The relationship between the sea surface wave structure and the resulting modulation in observed volume fluorescence and Raman backscatter is not understood and is currently under investigation. This relationship is illustrated in Fig. 4 which shows profiles of the peak backscattered Raman signal strength and the sea surface elevation, both plotted as a function of time for an expanded segment of Pass 2 over the LaRosa slick presented in Fig. 2. Both parameters have been filtered with an 11-point moving average. The sea surface elevation was determined by subtracting the mean slant range measurement acquired by the AOL altimeter from individual slant range measurements and inverting the results such that the peaks represent wave crests and conversely the depressions represent

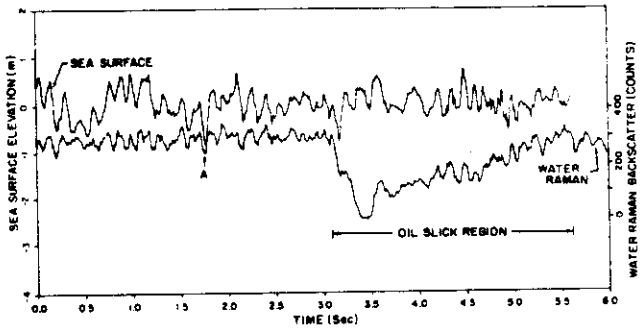

Fig. 4. High correlation of water Raman backscatter with sea surface elevation. The spatial phase lag of the Raman is evident but more easily seen at *A*. The correlation persists even over the ocean surface region covered by the oil slick.

wave troughs. Vertical aircraft motion has not been removed from the data, however, this motion is of little consequence in the following discussion. The aircraft vertical motion is normally removed by a recently developed technique[28] utilizing a vertical accelerometer, however, this accelerometer was not onboard during this mission. The correspondence (outside the oil slicks themselves) of higher Raman signal to wave crests and lower Raman signal to wave troughs persisted throughout the oil spill data sets and, as will be seen, also exists in our more recently acquired depth-resolved water Raman backscattered signal discussed in the concluding portion of this section. Also, note particularly the apparent phase shift between the Raman signal peak and the wave crests in a number of cases while there are a few exceptions. Variations in Raman backscatter signal from the ocean volume appear to lag corresponding variations in the sea surface record. This is quite evident in Fig. 4 at the position *A* where the local Raman depression appears to lag the wave trough. It should also be noted that the detection of the ocean surface is dominated by Fresnel reflection with some Mie backscatter components from the ocean volume while the Raman backscattered signal is strictly volumetric. As indicated previously, a detailed study of the relationship between volumetric Raman backscatter (and on-wavelength surface return power) and sea surface elevation is in progress in our laboratory.

Figure 5 shows the AOFSCE at 500 nm of both oil types plotted as a function of oil film thickness. The upper cluster of data points is taken entirely from Pass 4 over the Murban crude shown in Fig. 3. The lower cluster of data points was obtained on the first 4 passes over the LaRosa crude. The computation of AOFSCE, of course, requires fluorescence measurement and, as can be observed in Fig. 2, the fluorescence obtained over the LaRosa slick was confined to a relatively low number of points on a single pass. Thus, by necessity the results of several passes were combined.

The computed conversion efficiency at ~500 nm for the Murban crude oil shown in Fig. 5(a) can be seen to be approximately the same for all thicknesses greater than ~2μm. The reader is reminded that η_f and thickness are connected through the Raman ratios since the thickness is

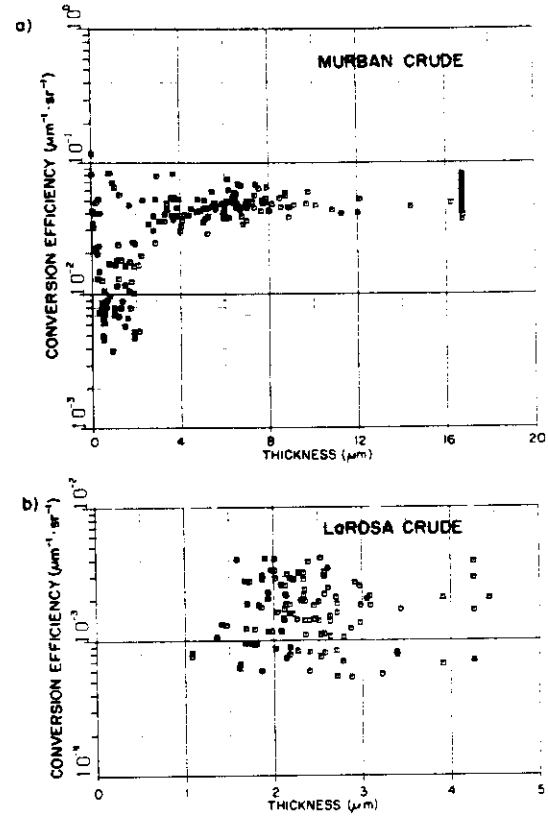

Fig. 5. (a) Oil fluorescence conversion efficiency of Murban crude oil as a function of the film thickness. (b) Oil fluorescence conversion efficiency of LaRosa crude oil as a function of the film thickness.

$$d = -\frac{1}{\kappa_e + \kappa_r} \ln\left(\frac{R'}{R}\right).$$

Although the theoretical model should recover the same conversion efficiency for all thicknesses, the fluorescence yield is apparently too low for films <2 μm thick. This is especially evident for the more fluorescent Murban crude. A minimum limit for the AOFSCE application was not totally unexpected since the calculations of Kung and Itzkan[8] showed that the film should be >0.5 μm to attain a conversion efficiency within a factor of 2 accuracy using a lidar having instrument parameters similar to the AOL.

The results obtained in the computation of conversion efficiencies for LaRosa crude oil shown in Fig. 5(b) are not as succinct. All fluorescence responses below 1 count above background were edited, thus no conversion efficiencies below ~1 μm are shown. In addition, there is considerable spread in the cluster of conversion efficiencies throughout the range from 1 to 4.5 μm, however this variance is to be expected in conditions where the peak fluorescence response approaches the detection limitations of the instrumentation. This aspect will be addressed and amplified in the concluding portion of this paper and is not considered a serious obstacle to the eventual utilization of the AOFSCE technique. The conversion efficiencies of the two oils are separated by approximately ×30 for all thicknesses greater than ~2-μm. This field result is in poor

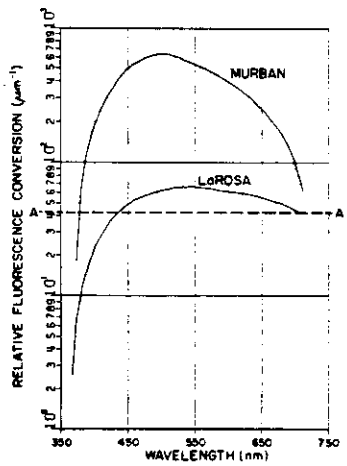

Fig. 6. Relative oil fluorescence conversion efficiency of Murban and LaRosa crudes as measured in the laboratory. An airborne system detection sensitivity level denoted as A in the figure will account for the apparent difference in conversion efficiency as measured in the field.

agreement with the laboratory measurements of the relative fluorescence intensities already reported.[9,21] However, we do not think that the theoretical model is necessarily at fault. Instead, the instrument sensitivity limit appears to have been reached in the case of the LaRosa crude oil overpasses. Ignoring the aging of the slicks (the Murban was overflown 15 min after deployment, while the LaRosa passes were overflown between 20 and 100 min after spillage), the disparity between the laboratory and field measurements can be explained by referring to Fig. 6. This figure shows relative fluorescence emission spectra obtained from laboratory measurements made on Murban and LaRosa crude oils. The Murban crude is seen to yield approximately ×10 higher fluorescence than the LaRosa. However, if a detection limit is encountered, the apparent ratio of peak intensities is changed accordingly. For the arbitrary detection limit shown by level A in Fig. 6, the ratio of the peak intensity at ~500 nm is seen to be ×30.

The results of these field experiments indicate that several recommendations should be considered in planning and conducting future airborne missions of these kinds. (a) To test the AOFSCE technique (not test the observing instrument), crude oils having fluorescence conversion efficiencies differing by only ×2 or ×3 should be utilized. (b) The weakest fluorescing oil selected should produce responses above the minimum detection limit of the lidar system used for the experiment. Accordingly, means should be provided in the lidar to maintain linearity and avoid saturation in the detection system when the highly fluorescent oils are being measured. In short, the dynamic range of the lidar system should comfortably encompass the oil spill targets being sensed.

Laboratory techniques for supporting airborne AOFSCE measurements are still under development and will be reported in a future publication. The fact that reasonably quantifiable estimates of oil fluorescence efficiencies can be obtained over a considerable range of thicknesses below optically opaque thicknesses is the practical utility of the AOFSCE technique. Furthermore, the ability to recover AOFSCE values in the presence of interfering background or Gelbstoff fluorescence gives the technique added value. The lower limits of thickness where the technique is applicable for each oil can be extended downward with increasing laser excitation power and/or improved instrument detection and spectral resolution. Recent modifications to the AOL since the 1978 oil spill show promise for improving these aspects of our instrument. These elements will also be addressed in the concluding portion of this paper.

B. Water Raman Conversion Field Experiments

Airborne Raman conversion experiments were conducted in May 1981 during the course of a field mission denoted as the Nantucket Shoals Phytoplankton Dynamics Experiment. The independent measurement of water attenuation properties is a continuing need in all our other airborne oceanographic applications, and the demonstration of the general feasibility of the remote measurement of water clarity parameters using depth-resolved water Raman backscatter was one of the primary objectives of the initial NASA involvement in the shoals experiment. The AOL instrument was configured in the bathymetry mode for the water column depth-resolved Raman experiments. Two laser transmitters were used at 532 and 422.6 nm on separate missions. The resulting 3300-cm^{-1} Raman emissions then occur at 650 and 493.5 nm. For simplicity, only the results from the 422.6-nm laser are discussed in this paper.

The 420–430-nm spectral region for one of the laser wavelengths was selected to take advantage of the water transmission at both the laser and Raman spectral lines. Additionally, this blue spectral region was ideal and necessary for directly exciting the chlorophyll a during phytoplankton mapping experiments which were conducted during the same mission. Specifically, the 422.6-nm laser wavelength was chosen because of the availability of a large diameter 493.5-nm interference filter centered at the Raman spectral line. A Kodak No. 4 filter was used in series with the 493.5-nm interference filter to provide additional blocking of the 422.6-nm on-wavelength laser backscatter. The 422.6-nm output was obtained from a Lambda Physik dye laser being pumped with a 308-nm XeCl excimer laser. The various transmitter/receiver parameters are summarized in Table I.

The 493.5-nm depth-resolved water Raman data were obtained on 9 May 1981, NE of Nantucket Island. Supporting spectral diffuse attenuation coefficient observations were obtained from a Brookhaven National Laboratories research vessel (Onrust) using a multiwavelength spectral radiometer (Biospherical Instruments). Measurements were obtained at depth intervals of ~2 m and for twelve wavelengths between 410 and 694 nm. The observations obtained from the research vessel at their Station 5, which we overflew, and at nearby stations indicated that the watermass was well

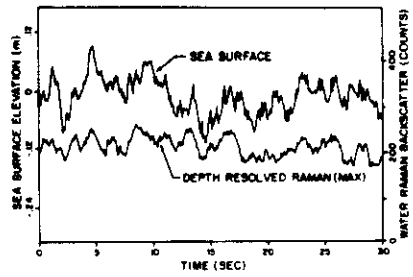

Fig. 7. High correlation between the depth-resolved water Raman and the sea surface elevation. The sea surface is derived from range data obtained from the leading edge of the depth-resolved water Raman return pulse.

mixed with little horizontal or vertical variation in the diffuse attenuation coefficient. The mean value of the diffuse attenuation coefficient at Station 5 in the upper 20 m of the water column was determined to be 0.23 m^{-1} at 441 nm, while the surface chlorophyll *a* concentration was measured to be 1.3 μg/liter. The airborne lidar results likewise indicated little change in the mean Raman backscattered signal in the vicinity of Station 5.

The pulse-to-pulse depth-resolved water Raman backscattered signal has considerable variation which is correlated with sea surface elevation variability as was the case with the integrated water column Raman backscattered signals obtained during previously discussed 1978 oil spill data. Figure 7 is a cross-sectional or time-series plot of the sea surface elevation and the peak water Raman backscattered signal amplitude for a 30-sec period as the aircraft passed near the research vessel. The data have been smoothed with an 11-point moving average filter. The high correlation of the volumetric signals and the surface wave structure should be noted. The ocean surface height was determined by the same method described in the discussion of Fig. 4. Similarly the aircraft motion has not been removed from this relatively short segment of data since it does not significantly affect the surface elevation considerations being discussed. It should be noted that the slant range measurement used in the computation of the sea surface elevation was derived from the leading edge of the received Raman backscattered signal and not from the on-wavelength laser return signal as was the case in the oil spill data. Thus the slant range measurement was derived from the signal received from the upper water volume. The relationship between the ocean surface wave structure and our volumetric backscatter signals is not completely understood and is currently under investigation. We consider the resolution of this problem to be both fundamental and essential to the refinement of all oceanographic lidar investigations. Our future studies of this sea surface modulation of water column coupling will include surface slopes and local roughness as well as laser incidence angle.

Since the water Raman signal possessed significant pulse-to-pulse amplitude variation, we selected only those pulses falling within 20 counts of the mean amplitude of the Raman backscattered signal for further analysis of the depth resolution of the water Raman signal. These return signals were subsequently averaged to produce a single waveform for comparison with calibration data obtained during a ground test conducted immediately following the flight experiment. The ground test consisted of radiating a flat target board with the system configured to temporally resolve the on-wavelength laser backscattered signal. (The authors recognize that the photomultiplier temporal response is wavelength dependent; however the effect is not well quantified.[29,30]) During the ground test the return pulse amplitudes were adjusted using the receiver field of view (FOV) to produce a similar amplitude distribution to that obtained from water Raman backscatter during the flight experiment.

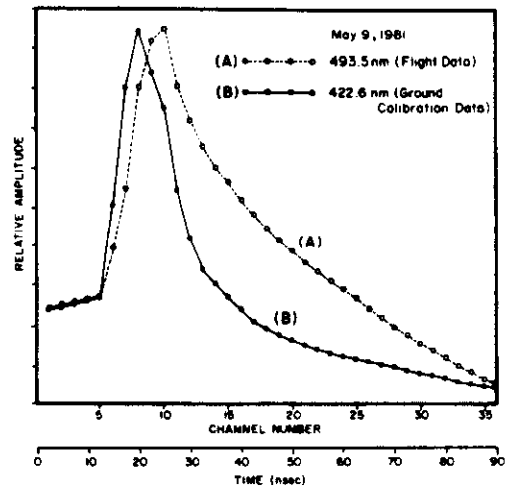

Fig. 8. (a) Depth-resolved water Raman backscatter data at 493.5 nm obtained during field experiments on Nantucket Shoals. (b) System temporal response calibration data at 422.6 nm obtained from a flat target immediately following the flight mission.

These pulses were then averaged to produce a mean system temporal response calibration waveform. The waveforms from the field experiment and ground test are shown in Fig. 8. A comparison between these waveforms indicates that the water Raman waveform shows the requisite time decay stretching that exceeds the flat-target system response. These results were very encouraging in that the feasibility for acquisition of depth-resolved Raman data from low-flying aircraft platforms has been demonstrated. Initial attempts to satisfactorily deconvolve[31,32] the system response from the depth-resolved Raman data as yet has been only marginally successful. The deconvolution process has been hampered by an amplitude dependent droop visible in both the Raman and calibration data in Fig. 8. This droop was caused by a video amplifier and delay line which follow the photomultiplier detector. A new amplifier and delay line have since been installed and opportunities to secure new airborne field data are being sought. Additionally, extensive ground tests of the hardware and deconvolution software are now in progress. Future experiments will utilize in-flight

targets such as a nearby beach or other flat land area to obtain the system response. This will help reduce system drift that can possibly occur when too much time elapses between the acquisition of the experiment data and the required system response calibration data.

V. Conclusions

The results of our investigations have demonstrated that consistent AOFSCE values can be obtained from oil films on the ocean surface with an airborne laser fluorosensor over a considerable range of thicknesses provided the fluorescence of the oil is above the minimum detection limit of the fluorosensor receiver. During the 1978 experiments reported here, the minimum thickness for obtaining consistent AOFSCE values was ~2 μm, somewhat above the 0.5-μm thickness suggested by the calculations of Kung and Itzkan.[8] Likewise, the spread and the magnitude of AOFSCE measurements from individual laser pulses are affected by the available fluorescence from the oils themselves relative to the detection limit or sensitivity of the system. As could be seen in the results from the LaRosa oil spill in our data, the calculation of AOFSCE for oils that have maximum fluorescence yields at or near the minimum detection limit of the lidar system can give erroneous absolute values. The sensitivity of a lidar system, however, can be altered by improving the optical components or effectively by increasing laser power, thus the 2-μm minimum obtained during these experiments should not be viewed as a physical lower bound or limitation.

The effective application of AOFSCE will require reasonably precise spectral calibration of the lidar receiver. Unfortunately, at the time of the 1978 oil spill we did not have techniques developed to perform such a calibration. As a result we were not able to determine the relative sensitivity of the Raman channel relative to the peak fluorescence channel, thus the absolute magnitude of the AOFSCE values shown may be somewhat in error. Recent techniques for calibrating our spectrometer with pulsed calibration sources, the addition of individual software driven voltage controls for the spectral channels, and the acquisition of an excimer laser with 100× more power than was available for 1978 oil spill experiments have all enhanced the capability of the AOL for performing oil spill investigations.

Separate airborne lidar experiments were also conducted to demonstrate measurement of the water Raman conversion efficiency for converting the fluorescence to absolute values. We were successful only in showing that no major practical obstacles apparently exist in performing the airborne water Raman conversion measurements. For example, the water clarity encountered during our field tests yielded adequate signal strength to allow Raman measurement as a function of depth. Unfortunately, airborne Raman (and immediate postmission ground calibration) pulse distortion caused by the video amplifiers and delay lines made satisfatory deconvolution a difficult task. Deconvolution techniques and software have varying degrees of sensitivity to SNR as well as bias in the waveforms. The available hardware and software analytical techniques have not been exhausted. On the contrary several options are available for additional experiments. We conclude that the airborne Raman conversion feasibility is still an open question but that the prospects for success are very positive for fully demonstrating airborne Raman conversion feasibility.

The potential utility of using AOFSCE to differentiate oil film types is especially promising when combined with spectral fluorescence correlation procedures such as the one recently reported by O'Neil *et al.*[9] Techniques involving spectral recognition are somewhat hampered when applied to slicks of varying thicknesses below the critical or minimum detectable optical thickness. A technique which incorporated AOFSCE within the spectral correlation analysis framework could get consistent results over films that were not opaque and within coastal waters with interfering Gelbstoff fluorescence from dissolved organic matter.

The authors wish to thank all those who composed the team responsible for this work. Space does not allow us to list completely the individuals who were directly or indirectly involved in the success of these experiments. We would like to thank the Aeronautical Programs Branch for the aircraft support; JBF Scientific Corp., American Petroleum Institute, and NOAA for their oil spill experiment leadership and contributions; the Brookhaven National Laboratory for water clarity and chlorophyll measurements; Marine Environments Branch and Electromagnetics Research Branch, both of NASA's Langley Research Center. Appreciation is expressed to W. Stanley Wilson and members of the NASA Headquarters Oceanic Processes Branch for their programmatic support and encouragement of this work.

References

1. E. P. Myers and C. G. Gunnerson, "Hydrocarbons in the Oceans," NOAA Marine Ecosystems (MESA) Analysis Program Special Report, Boulder, Colo., Apr. 1976.
2. O. I. Abramov, V. I. Yeremin, L. I. Lobov, and V. V. Polovinko, Izv. Acad. Sci. USSR Atmos. Oceanic Phys. **13**, 232 (1977).
3. D. M. Rayner and A. G. Szabo, "A Study of the Potential of Time-Resolved Laser Fluorosensors," Report BY-76-2 (RC), National Research Council of Canada, Ottawa, Canada, Nov. 1976.
4. H. Visser, Appl. Opt. **18**, 1746 (1979).
5. J. F. Fantasia and H. C. Ingrao, "The Development of an Experimental Airborne Laser Remote Sensing System for the Detection and Classification of Oil Spills," in *Proceedings, Ninth International Symposium on Remote Sensing of the Environment, 15–19 Apr. 1974* (Environmental Research Institute of Michigan, Ann Arbor, 1974), Vol. 3, pp. 1711–1745.

6. J. F. Fantasia and H. C. Ingrao, "The Development of an Experimental Airborne Laser Remote Sensor for Oil Detection and Classification of Spills," Final Report CG-D-86-75, U.S. Department of Transportation, Cambridge, Mass., Feb. 1975.
7. R. Horvath, W. L. Morgan, and S. R. Stewart, "Optical Remote Sensing of Oil Slicks: Signature Analysis and Systems Evaluation," Project 724104.2/1, Willow Run Laboratories, U. Michigan, Ann Arbor, Oct. 1971.
8. R. T. V. Kung and I. Itzkan, Appl. Opt. **15,** 409 (1976).
9. R. A. O'Neil, L. Buja-Bijunas, and D. M. Rayner, Appl. Opt. **19,** 863 (1980).
10. H. H. Zwick, R. A. Neville, and R. A. O'Neil, "A Recommended Sensor Package for the Detection and Tracking of Oil Spills," in *Proceedings, EARSeL-ESA Symposium, NOSS, Norway, 19–20 May 1981* (ESA Publication, Application of Remote Sensing Data on the Continental Shelf, SP-167, July 1981).
11. R. W. Holmes, Limnol. Oceanogr. **15,** 688 (1970).
12. J. G. Shannon, SPIE J. **64,** 3 (1975).
13. G. S. Ofelt, "Relationship Between Beam and Diffuse Attenuation Coefficients in the Lower Chesapeake Bay Area," Technical Report 32, prepared by Old Dominion U., Norfolk, Va. under Master Contract Agreement NAS1-14193 for NASA Langley Research Center, Oct. 1976.
14. H. R. Gordon and A. W. Wouters, Appl. Opt. **17,** 3341 (1978).
15. M. Bristow, D. Nielsen, D. Bundy, and R. Furtek, Appl. Opt. **20,** 2889 (1981).
16. R. W. L. Thomas and G. C. Guenther, "Theoretical Characterization of Bottom Returns for Bathymetric Lidar," in *Proceedings, International Conference on Lasers '78,* Society of Optics and Quantum Electronics, Orlando, Fla. 11–15 Dec. 1978.
17. H. R. Gordon, Appl. Opt. **21,** 2996 (1982).
18. L. R. Poole and W. E. Esaias, Appl. Opt. **21,** 3756 (1982).
19. R. B. Slusher and V. E. Derr, Appl. Opt. **14,** 2116 (1975).
20. C. H. Chang and L. A. Young, "Seawater Temperature Measurement from Raman Spectra," Final Technical Report, Contract N62269-72-C-0204, Advanced Research Projects Agency Order 1911 to Avco Everett Research Laboratory, Everett, Mass. (July 1972).
21. F. E. Hoge and R. N. Swift, Appl. Opt. **19,** 3269 (1980).
22. F. E. Hoge and R. N. Swift, Appl. Opt. **20,** 1191 (1981).
23. F. E. Hoge and R. N. Swift Appl. Opt. **20,** 3197 (1981).
24. F. E. Hoge and R. N. Swift "Application of the NASA Airborne Oceanographic Lidar to the Mapping of Chlorophyll *a* and Other Organic Pigments," in NASA Conference Publication 2188, NOAA/NEMP III 81-ABCDFG0042, Chesapeake Bay Plume Study (Superflux 1980), J. W. Campbell and J. P. Thomas, Eds., Jan. 1981.
25. F. E. Hoge, R. N. Swift, and E. B. Frederick, Appl. Opt. **19,** 871 (1980).
26. C. D. McAuliffe, J. C. Johnson, S. H. Green, G. P. Caneveri, and T. D. Searl, Environ. Sci. Technol. **14,** 1509 (1980).
27. W. F. Croswell, J. C. Fedors, F. E. Hoge, R. N. Swift, and J. C. Johnson, "Ocean Experiments and Remotely Sensed Images of Chemically Dispersed Oil Spills," IEEE Trans. Geosci. Remote Sensing **GE-21,** No. 1, (1983), accepted for publication.
28. W. B. Krabill, NASA; personal communication; paper in preparation for publication as NASA Technical Memorandum.
29. P. Wahl, J. C. Auchet, and B. Donzel, Rev. Sci. Instrum. **45,** 28 (1974).
30. A. E. McKinnon, A. G. Szabo, and D. R. Miller, J. Phys. Chem. **81,** 1564 (1977).
31. J. M. Mendel, IEEE Trans. Geosci. Remote Sensing, **GE-19,** 161 (1981).
32. J. A. Irvin and T. I. Quickenden, Rev. Sci. Instrum. **52,** 191 (1981).